Catalysis Science & Technology

PAPER

View Article Online
View Journal | View Issue



Cite this: *Catal. Sci. Technol.*, 2015, 5, 572

# Multifunctional mesoporous silica-supported palladium nanoparticles for selective phenol hydrogenation in the aqueous phase

Fengwei Zhang*[a] and Hengquan Yang*[ab]

Received 10th August 2014,
Accepted 18th September 2014

DOI: 10.1039/c4cy01036a

www.rsc.org/catalysis

A simple, efficient and recoverable palladium-based catalyst was successfully prepared by immobilizing palladium nanoparticles (Pd NPs) over hydrophobic core–hydrophilic shell structured mesoporous silica microspheres. The obtained catalyst was characterized by transmission electron microscopy (TEM), $N_2$ adsorption–desorption, Fourier-transform infrared spectroscopy (FTIR), thermogravimetric analysis (TGA) and X-ray photoelectron spectroscopy (XPS). The as-prepared catalyst could rapidly convert phenol to cyclohexanone with 98.5% conversion and 97.1% selectivity under mild reaction conditions in the aqueous phase (1 atm $H_2$, 80 °C, 3 h). The excellent catalytic performance of the Pd/MS-$C_3$@MS-$NH_2$ catalyst was probably attributed to the enhanced synergistic effect between highly dispersed Pd NPs and significantly decreased phenol mass transfer resistance. In addition, it could be easily recovered by centrifugation and reused 5 times without any significant loss in activity and selectivity.



## Introduction

Core–shell structured multifunctional mesoporous materials have recently attracted significant attention owing to their unique characteristics, such as high specific surface area, controllable pore structure, narrow pore size distribution, and versatile surface functionalization.[1–5] Thus, they are generally regarded as an ideal candidate for catalysis, adsorption, separation, energy storage and conversion, drug delivery and optics.[6–12] Among them, as far as catalyst supports are concerned, great progress has been made in their functionalization, and the developed heterogeneous catalytic systems displayed extremely high catalytic activity, selectivity and stability in a variety of important organic transformations.[13–20] For example, Suzuki *et al.* first reported the $SO_3H$ core–hydrophobic shell structured mesoporous silica microspheres through the co-condensation/expansion method, which exhibited enhanced catalytic activity for the condensation reaction of 2-methylfuran and acetone. They found that the obvious enhancement in catalytic activity due to the incorporation of hydrophobic groups was only achieved with core–shell structure, and little enhancement was observed in a randomly distributed structure.[21] Yang *et al.* have also successfully prepared a yolk–shell multifunctional nanoreactor with basic core ($-NH_2$) and acidic shell ($-SO_3H$), which showed excellent catalytic performance in deacetalization–Henry cascade reaction.[22]

As is well-known, the hydrogenation of phenol is one of the effective methods for the preparation of cyclohexanone, which serves as an important intermediate in the synthesis of caprolactam and adipic acid.[23] The phenol hydrogenation route is generally undertaken through one- or two-step processes.[24] The two-step process involves hydrogenation of phenol to cyclohexanol followed by dehydrogenation to cyclohexanone.[25] The one-step selective phenol hydrogenation to cyclohexanone, in contrast, is more advantageous in the perspective of energy efficiency and operation cost. Recently, considerable research has been devoted to the development of highly active heterogeneous catalysts for one-step selective phenol hydrogenation.[26] In particular, Han and co-workers have reported the synthesis of an unprecedented commercially available heterogeneous palladium and Lewis acid combined catalyst, which was carried out at 50 °C under 10 atm of $H_2$ for liquid-phase phenol hydrogenation.[27] However, the environmentally unfriendly co-catalysts and organic solvents were indispensable for the reaction process as the reaction pressure was relatively higher.

To overcome these problems, palladium nanoparticles supported on a variety of organic and inorganic materials, such as polymers,[28] mpg-$C_3N_4$,[29] N-doped ordered mesoporous carbon (NOMC),[30] carbon nanotubes (CNTs),[31] and carbon nanofibers (CNFs),[32] have been developed and used to catalyze the hydrogenation of phenol in the aqueous phase. Nevertheless, the separation and recycling of the polymer-supported catalyst were relatively complicated and

[a] *Institute of Crystalline Materials, Shanxi University, Taiyuan 030006, PR China. E-mail: fwzhang@sxu.edu.cn, hqyang@sxu.edu.cn; Tel: +86 351 7016082*
[b] *School of Chemistry and Chemical Engineering, Shanxi University, Taiyuan 030006, PR China*

the Pd NPs were inclined to aggregate due to the high surface energy. In addition, the preparation procedures of these types of solid supports usually involve multiple steps of preparation, high pyrolysis temperature and environmentally unfriendly reactants, which consume a considerable amount of time and energy. It is also very important to have the ability to scale up the synthesis for the preparation of large quantities of materials. Therefore, the development of a more facile and greener heterogeneous catalyst with excellent phenol conversion and selectivity is still a great challenge. To our knowledge, there is no report of direct selective hydrogenation of phenol to cyclohexanone over easily recyclable multifunctional core–shell structured mesoporous silica in the aqueous phase. Herein, we report a novel hydrophobic core/hydrophilic shell structured mesoporous silica immobilized Pd NP catalyst, which acts as a highly active, water-tolerant, and easily recyclable catalyst for selective phenol hydrogenation. More importantly, it can be easily recycled and used repetitively more than 5 times without loss of catalytic efficiency.

# Experimental

### Materials

Palladium(II) acetate ($Pd(OAc)_2$, ≥97%), tetramethyl orthosilicate (TMOS, 98%) and sodium hydroxide (NaOH) were purchased from Sinopharm Chemical Reagent Co., Ltd. Sodium borohydride ($NaBH_4$, 98%), (3-aminopropyl)trimethoxysilane (APTMS) and *n*-propyltrimethoxysilane ($C_3$TMS) were obtained from Aladdin Chemical Reagent Co., Ltd. Cetyltrimethylammonium chloride (CTAC, 99%) was purchased from Nanjing Robiot Co., Ltd. All other chemicals were of analytical grade and were used without any further purification.

### Preparation of hydrophobic core–hydrophilic shell mesoporous silica

Hydrophobic core–hydrophilic shell mesoporous silica was prepared according to the method previously described by Suzuki *et al.* with some modification.[21] Specifically, 3.52 g of CTAC and 2.5 mL of NaOH (1.0 mol $L^{-1}$) were dissolved in a mixture solution of 400 mL of deionized water and 500 mL of methanol, and then 1.20 g of TMOS and 0.25 g of $C_3$TMS were added into the above solution with vigorous stirring at room temperature. After 1 h of pre-hydrolysis, 1.20 g of TMOS and 0.20 g of APTMS were slowly added to the suspension. After 8 h of continuous stirring, the obtained white precipitate was filtered and washed thoroughly with deionized water and ethanol and dried at 100 °C for 6 h. To remove the surfactant, the as-synthesized material was dispersed in a 100 mL ethanol solution containing 1.5 mL of concentrated HCl and the mixture was stirred at 80 °C for 12 h. The resulting material was designated as MS-$C_3$@MS-$NH_2$. As a control, the MS@MS-$NH_2$ and MS-$NH_2$@MS-$C_3$ were prepared under the same procedure except no $C_3$TMS was added into the synthesis process and in turn the order of adding.

### Loading of Pd NPs on hydrophobic core–hydrophilic shell mesoporous silica

To a stirred suspension of MS-$C_3$@MS-$NH_2$ (1.0 g) in 30 mL of deionized water was added 65 mg of $Pd(OAc)_2$. After stirring for 4 h (the amount of $Pd(OAc)_2$ adsorbed onto the solid materials was calculated from the UV-Vis spectra) 20 mL of $NaBH_4$ (120 mg) was slowly added and the suspension was stirred for another 2 h. The suspension was centrifuged and washed several times with deionized water and ethanol, resulting in Pd/MS-$C_3$@MS-$NH_2$ (the loading amount of Pd was 3.12 wt%).

### Pd/MS-$C_3$@MS-$NH_2$ catalysts for selective phenol hydrogenation

In a typical experiment, 80 mg of the catalyst (0.025 mmol), 0.5 mmol of phenol and 3 mL of deionized water were added into the reaction vessel. The vessel was sealed and purged three times with hydrogen to remove the air at room temperature. Then, hydrogenation was performed at 80 °C under 1 atm $H_2$ for 3 h. After completion of the reaction, the products were extracted with ethyl acetate, followed by analysis using an Agilent 7890A gas chromatograph, and the products were identified by comparison with authentic samples.

### Recycling of the Pd/MS-$C_3$@MS-$NH_2$ catalyst

The recyclability of the Pd/MS-$C_3$@MS-$NH_2$ catalyst was tested for phenol-selective hydrogenation in the aqueous phase under the same reaction conditions as described above. After each run of reaction, the catalyst was separated from the reaction mixture by centrifugation, washed thoroughly with ethanol, dried at 60 °C for 2 h, and then reused directly for the next run.

### Characterization

Transmission electron microscopy (TEM) was performed using a FEI Tecnai G2 F20S-Twin with an accelerating voltage of 200 kV. For sample preparation, the powders were dispersed in ethanol by sonication, and one drop of the solution was dropped onto a microgrid. $N_2$ adsorption–desorption isotherms were obtained with an ASAP2020 analyzer. Before measurement, samples were degassed under vacuum at 373 K for 6 h. The surface area of the samples was calculated by the Brunauer–Emmet–Teller (BET) method, and the pore volume and pore size distribution were calculated using the Barrett–Joyner–Elmer (BJH) model. Thermogravimetric analysis (TGA) was performed using a SETARAM Evolution 16/18 apparatus. The samples were heated on an alumina pan from 25 °C to 800 °C at a heating rate of 10 °C $min^{-1}$ under nitrogen. Fourier transform infrared (FTIR) spectra were obtained using a Nicolet NEXUS 670 spectrophotometer (frequency range from 4000 to 500 $cm^{-1}$) with KBr pellets. X-ray photoelectron spectra (XPS) was obtained with the PHI-5702 instrument and the C1S line at 286.6 eV was used as the binding energy reference.

## Results and discussion

The synthesis route of the hydrophobic core–hydrophilic shell structured Pd/MS-$C_3$@MS-$NH_2$ catalyst is illustrated in Scheme 1. Firstly, the hydrophobic core was prepared through the co-condensation of TMOS and $C_3$TMS in the presence of CTAC in an alkaline methanol solution. Secondly, after a certain time of pre-hydrolysis and condensation, a mixture of TMOS and APTMS was added to the above suspension to form a layer of hydrophilic shell. The resultant materials were extracted with hot acidic alcohol solution to remove CTAC. Thirdly, palladium nanoparticles were immobilized on the MS-$C_3$@MS-$NH_2$ microspheres by impregnation and subsequent reduction.

The respective TEM images of MS-$C_3$@MS-$NH_2$, Pd/MS-$C_3$@MS-$NH_2$, Pd/MS@MS-$NH_2$ and Pd/MS-$NH_2$@MS-$C_3$ are shown in Fig. 1. From the TEM image of MS-$C_3$@MS-$NH_2$ (Fig. 1a), highly uniform microspheres with an average diameter of 340 nm, a shell thickness of 30 nm and perpendicularly oriented channels about 2.7 nm in diameter can be seen. For Pd/MS-$C_3$@MS-$NH_2$ and Pd/MS@MS-$NH_2$ catalysts (Fig. 1b and c), the products were composed of uniform mesoporous microspheres with a particle size of 350 nm, which were similar to those of MS-$C_3$@MS-$NH_2$ microspheres. Additionally, it can be clearly seen that most of the palladium nanoparticles with particle sizes of about 5.8 nm for Pd/MS-$C_3$@MS-$NH_2$ and 5.4 nm for Pd/MS@MS-$NH_2$ were uniformly dispersed on the surface of the multifunctional core–shell structured mesoporous silica. However, the Pd NPs were poorly distributed on the surface of the Pd/MS-$NH_2$@MS-$C_3$ catalyst (Fig. 1d) and they were inclined to aggregate into larger particles (about 8.1 nm).

Scanning transmission electron microscopy (STEM) analysis of the Pd/MS-$C_3$@MS-$NH_2$ catalyst was performed to obtain more detailed information about the structure. As shown in Fig. 2, STEM demonstrated that the as-synthesized Pd/MS-$C_3$@MS-$NH_2$ catalyst has a typical core–shell structure, which was in agreement with the results of TEM measurement. EDX element mapping of the sample further showed the spatial distributions of Si, O, N and Pd in the Pd/MS-$C_3$@MS-$NH_2$ catalyst. The strong Si and O signals across the sphere confirmed the presence of mesoporous silica, while the N and Pd signals detected in the surface region clearly suggested that they were evenly distributed on the surface of core–shell structured mesoporous silica. Moreover, our previous XPS elemental analysis results also have shown that the –$NH_2$ groups were mainly concentrated in the shell for the Pd/MF@MN catalyst (Pd NPs supported on fluoro-functionalized core and amino-functionalized shell structured mesoporous silica).[16]

In the FT-IR spectra of MS-$C_3$@MS-$NH_2$ and Pd/MS-$C_3$@MS-$NH_2$ microspheres (Fig. 3A), the peaks around 3422 $cm^{-1}$, 1404 and 1072 $cm^{-1}$ were assigned to the surface-absorbed water molecules, C–H bending and Si–O–Si stretching modes, respectively. The bands at 2926 and 2847 $cm^{-1}$ can also be seen in these two materials, which should be attributed to the saturated C–H stretching vibrations of propyl and aminopropyl groups, respectively. Meanwhile, the presence of N–H symmetric bending vibration at 1633 $cm^{-1}$ further confirmed the existence of amine groups. The results demonstrate that propyl and amino groups were successfully incorporated into the mesoporous silica microspheres and in the IR spectrum of Pd/MS-$C_3$@MS-$NH_2$, almost no change occurs after immobilizing Pd NPs on the MS-$C_3$@MS-$NH_2$ microsphere

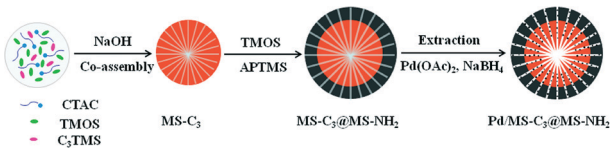


**Scheme 1** The synthesis procedure of the Pd/MS-$C_3$@MS-$NH_2$ catalyst.

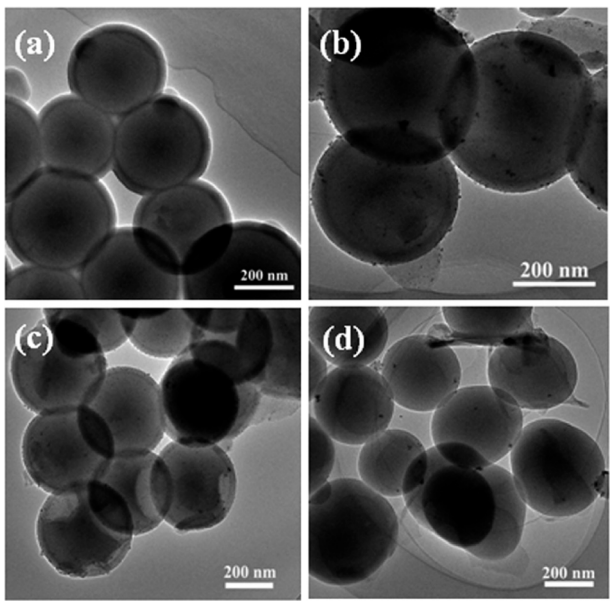


**Fig. 1** TEM images of (a) MS-$C_3$@MS-$NH_2$, (b) Pd/MS-$C_3$@MS-$NH_2$, (c) Pd/MS@MS-$NH_2$ and (d) Pd/MS-$NH_2$@MS-$C_3$.

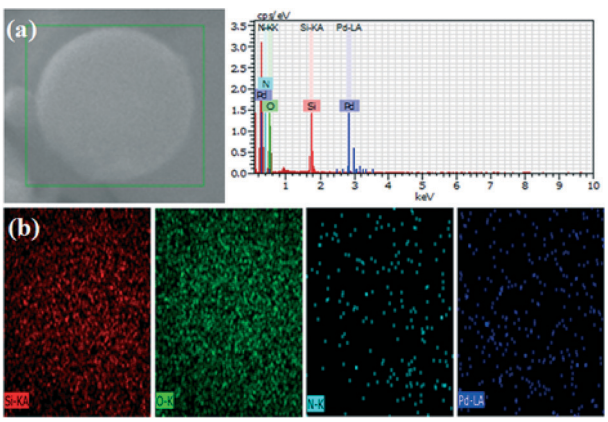


**Fig. 2** (a) Images of STEM and EDX of the Pd/MS-$C_3$@MS-$NH_2$ catalyst and (b) the corresponding elemental mapping of Si, O, N and Pd.

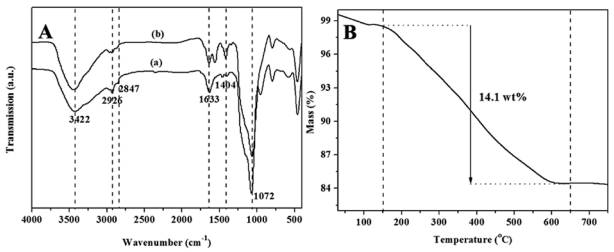


Fig. 3 (A) FTIR spectra of (a) MS-$C_3$@MS-$NH_2$ and (b) Pd/MS-$C_3$@MS-$NH_2$ and (B) the TGA curve of Pd/MS-$C_3$@MS-$NH_2$.

surface. The thermal stability of the Pd/MS-$C_3$@MS-$NH_2$ catalyst was investigated by TGA under nitrogen. As shown in Fig. 3B, the TGA curve of Pd/MS-$C_3$@MS-$NH_2$ exhibits 1.5 wt% weight loss at around 150 °C due to the loss of adsorbed water molecules, the second weight loss takes place above 150 °C, and about 14.1% weight loss was observed between 150 °C and 650 °C, indicating that propyl and amino groups were successfully incorporated into the mesoporous silica. The TGA curve of Pd/MS-$C_3$@MS-$NH_2$ further represents good thermal stability up to 150 °C.

The $N_2$ adsorption–desorption isotherms and the corresponding pore size distribution (inset) of MS-$C_3$@MS-$NH_2$ and Pd/MS-$C_3$@MS-$NH_2$ are shown in Fig. 4. Both the nitrogen adsorption and the desorption can be classified as type IV isotherms with a small hysteresis loop. The specific surface area, total pore volume and pore size of MS-$C_3$@MS-$NH_2$ were calculated to be 731 $m^2\ g^{-1}$, 0.375 $cm^3\ g^{-1}$ and 2.54 nm, respectively. The high specific surface area and well-developed mesoporous channels suggest that it was a good candidate as support for loading active Pd NPs. The specific surface area, total pore volume and pore size were 494 $m^2\ g^{-1}$, 0.258 $cm^3\ g^{-1}$ and 2.38 nm, respectively, after immobilizing Pd NPs on MS-$C_3$@MS-$NH_2$ microspheres, indicating that Pd loading had little effect on the specific surface area and pore size distribution of Pd/MS-$C_3$@MS-$NH_2$.

The catalyst was also characterized by XPS in order to ascertain the oxidation state of Pd in the catalyst. Fig. 5 shows the Pd 3d spectrum of the catalyst. It can be seen that the Pd binding energy of Pd/MS-$C_3$@MS-$NH_2$ presented two

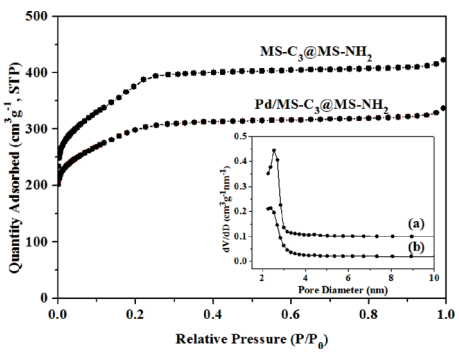


Fig. 4 Nitrogen adsorption–desorption isotherms and pore size distributions of (a) MS-$C_3$@MS-$NH_2$ and (b) Pd/MS-$C_3$@MS-$NH_2$.

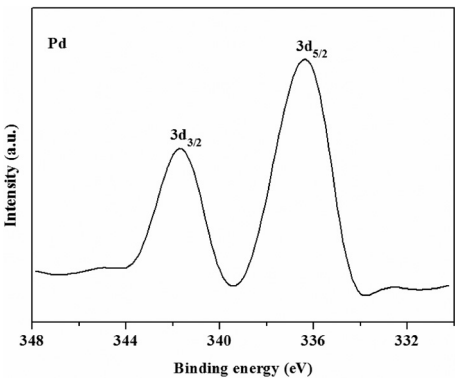


Fig. 5 XPS spectrum of the Pd/MS-$C_3$@MS-$NH_2$ catalyst.

sharp peaks centered at 341.6 and 336.4 eV, which were ascribed to Pd $3d_{3/2}$ and Pd $3d_{5/2}$, respectively. The results demonstrated that all of the Pd(II) species were completely converted into Pd(0) nanoparticles through chemical reduction with $NaBH_4$.

The catalytic activity of different heterogeneous catalysts was evaluated for the selective phenol hydrogenation and the results are summarized in Table 1. As can be seen, in the absence of the catalyst and in the presence of MS-$C_3$@MS-$NH_2$ at 80 °C for 6 h in the aqueous phase, no product was detected (Table 1, entries 1 and 2). For Pd/MS-$NH_2$@MS-$C_3$ and Pd/MS@MS-$NH_2$ catalysts, the reaction proceeds slowly with 38.2% and 78.8% phenol conversion and >99% and 98.7% cyclohexanone selectivity, respectively (Table 1, entries 3 and 4). As expected, when the reaction time increased from 3 h to 6 h, the conversion of phenol increased to 83.8% and >99%, while the selectivity for cyclohexanone decreased to 98.6% and 97.5%, respectively (Table 1, entries 5 and 6). It is worth mentioning that the reaction proceeds smoothly with 98.5% phenol conversion and 97.1% cyclohexanone selectivity in the presence of Pd/MS-$C_3$@MS-$NH_2$ within 3 h (Table 1, entry 7). Apparently, the hydrogenation rate of this new heterogenized catalyst was higher than that of its quasi-homogeneous counterpart (1 atm $H_2$, 90 °C, 16 h).[26a] The excellent catalytic performance of Pd/MS-$C_3$@MS-$NH_2$ was probably due to the hydrophilic shell being not only highly

Table 1 Selective hydrogenation of phenol to cyclohexanone by different catalysts[a]

| Entry | Catalyst | $T$ (°C) | $t$ (h) | Conv.[b] (%) | Sel.[b] (%) |
|---|---|---|---|---|---|
| 1 | — | 80 | 6 | — | — |
| 2 | MS-$C_3$@MS-$NH_2$ | 80 | 6 | — | — |
| 3 | Pd/MS-$NH_2$@MS-$C_3$ | 80 | 3 | 38.2 | >99 |
| 4 | Pd/MS@MS-$NH_2$ | 80 | 3 | 78.8 | 98.7 |
| 5 | Pd/MS-$NH_2$@MS-$C_3$ | 80 | 6 | 83.8 | 98.6 |
| 6 | Pd/MS@MS-$NH_2$ | 80 | 6 | >99 | 97.5 |
| 7 | Pd/MS-$C_3$@MS-$NH_2$ | 80 | 3 | 98.5 | 97.1 |

[a] Reaction conditions: 0.5 mmol of phenol, 80 mg of catalyst (0.025 mmol) and 3.0 mL of $H_2O$ under 1 atm $H_2$. [b] The conversion and selectivity were determined using an Agilent 7890A gas chromatograph.

dispersed and stabilized Pd NPs through amino groups but also beneficial to the uniform dispersion of the heterogeneous catalyst in water. Moreover, the hydrophobic core could rapidly concentrate phenol to the surroundings of Pd NP active sites. Along with phenol being hydrogenated to cyclohexanone, it constantly diffused into the aqueous solution from the mesoporous channel and avoided the further hydrogenation of cyclohexanone. Therefore, the catalyst can achieve the efficient, green and selective hydrogenation of phenol.

Fig. 6a shows the evolution of phenol conversion and cyclohexanone selectivity with reaction temperature. As can be seen, the conversion of phenol increased from 85.2% to 99.6% as the reaction temperature increased from 50 °C to 90 °C. Although the conversion of phenol increased rapidly from 50 °C to 80 °C, the selectivity for cyclohexanone reduced gradually. Notably, a further increase in reaction temperature hardly improved the phenol conversion, but the selectivity for cyclohexanone significantly decreased from 98.2% to 86.5%. The influence of reaction time on phenol conversion and cyclohexanone selectivity is shown in Fig. 6b. The reaction was accompanied by a rapid increase in phenol conversion and a slight decrease in cyclohexanone selectivity in the first 3 h, suggesting that phenol was mainly hydrogenated to cyclohexanone in the first step. With the further increase in reaction time (from 3 h to 8 h), the phenol conversion no longer increased and cyclohexanone selectivity decreased gradually (from 97.1% to 88.2%), illustrating that the conversion of cyclohexanone into cyclohexanol plays a vital role in the second step. The influence of the S/C molar ratio on the conversion of phenol and selectivity for cyclohexanone is shown in Fig. 6c. When the molar ratio of S/C (substrate/catalyst) was 80 : 1, the conversion of phenol was low due to the inadequate number of active sites. The conversion increased as the S/C molar ratio decreased from 80 : 1 to 20 : 1, and a conversion of 98.5% was achieved. However, the conversion hardly changed with a further decrease of the S/C molar ratio. Considering the cost of the catalyst and reaction rate, the suitable amount of the S/C molar ratio was 20 : 1. Based on the above results, the optimum conditions of selective phenol hydrogenation were obtained: reaction time 3 h, reaction temperature 80 °C and S/C molar ratio 20 : 1. Under the optimized conditions, the conversion of phenol could reach 98.5% and the selectivity for cyclohexanone could reach 97.1%.

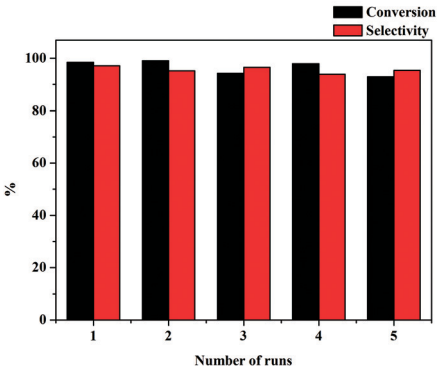


Fig. 7 Recycling tests of the Pd/MS-$C_3$@MS-$NH_2$ catalyst in selective phenol hydrogenation. Reaction conditions: 0.5 mmol of phenol, 3.0 mL of $H_2O$, 80 mg of catalyst, 1 atm $H_2$, 80 °C, 3 h.

Additional advantages of Pd/MS-$C_3$@MS-$NH_2$ prepared here were stability and ease of recycling because it can be facilely separated by centrifugation. Fig. 7 shows the recyclability of Pd/MS-$C_3$@MS-$NH_2$ for selective hydrogenation of phenol in the aqueous phase. It is worth mentioning that the catalyst still exhibited excellent catalytic activity even after running for more than five cycles. However, the slight decrease in phenol conversion with further recycle times should be due to the gradual leaching of Pd NPs from the catalyst surface (the Pd content in the catalyst was found to be 2.97 wt% based on ICP-AES analysis, indicating that *ca.* 4.8% of Pd was leached from the catalyst surface). The results clearly indicate that the high catalytic performance should be attributed to the small particle size and good dispersion of Pd NPs, high specific surface area and hydrophobicity of the core.

## Conclusion

In conclusion, a simple and environmentally friendly approach was reported for the synthesis of hydrophobic core–hydrophilic shell structured Pd/MS-$C_3$@MS-$NH_2$ nanocomposite catalysts, which exhibited superior catalytic activity and stability toward the selective hydrogenation of phenol in water. The reasons could be attributed to the

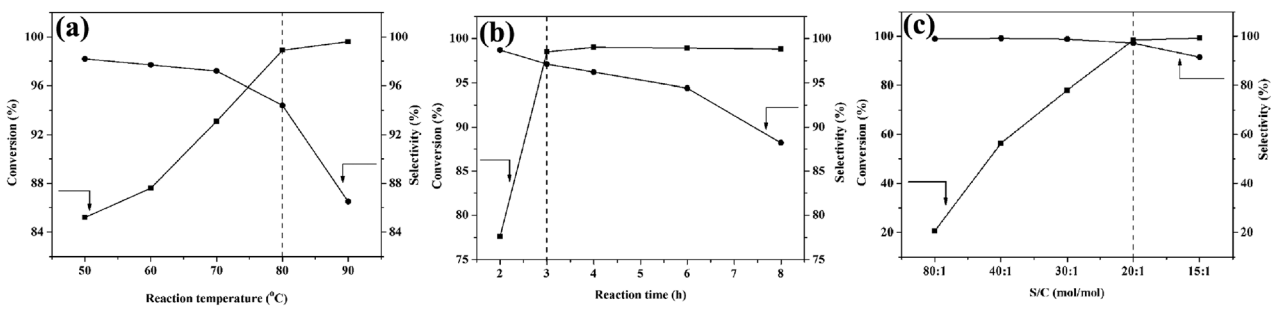


Fig. 6 Conversion of phenol and the selectivity for cyclohexanone as functions of (a) reaction temperature, (b) reaction time and (c) S/C molar ratio. Reaction conditions: 0.5 mmol of phenol, 3.0 mL of $H_2O$ and 1 atm $H_2$.

 

synergistic effect derived from binary organic functional groups since the amino groups promoted the uniform dispersion of Pd NPs inside the pore channels while the propyl groups decreased the diffusion limitation of phenol in water. Thus, it can be seen that this synthesis strategy provided a useful idea for the fabrication of other nanoparticle-supported catalysts with high specific surface area, ordered mesoporous channel and hydrophobic/hydrophilic functionality, which should be highly promising in diverse catalytic reactions.

## Acknowledgements

This work was supported by the Scientific Research Start-up Funds of Shanxi University (023151801002) and the National Natural Science Foundation of China (20903064, 221173137).

## Notes and references

1 D. Niu, Z. Ma, Y. Li and J. Shi, *J. Am. Chem. Soc.*, 2010, **132**, 15144–15147.
2 X. Liang, J. Li, J.-B. Joo, A. Gutiérrez, A. Tillekaratne, I. Lee, Y. Yin and F. Zaera, *Angew. Chem., Int. Ed.*, 2012, **51**, 8034–8036.
3 L. Xu, H.-G. Peng, K. Zhang, H. Wu, L. Chen, Y. Liu and P. Wu, *ACS Catal.*, 2013, **3**, 103–110.
4 Z. Li, L. Mo, Y. Kathiraser and S. Kawi, *ACS Catal.*, 2014, **4**, 1526–1536.
5 F. Zhang, X. Wu, C. Liang, X. Li, Z. Wang and H. Li, *Green Chem.*, 2014, **16**, 3768–3777.
6 (*a*) S. Ikurumi, S. Okada, K. Nakatsuka, T. Kamegawa, K. Mori and H. Yamashita, *J. Phys. Chem. C*, 2014, **118**, 575–581; (*b*) S. Okada, K. Mori, T. Kamegawa, M. Che and H. Yamashita, *Chem. – Eur. J.*, 2011, **17**, 9047–9051; (*c*) S. Okada, S. Ikurumi, T. Kamegawa, K. Mori and H. Yamashita, *J. Phys. Chem. C*, 2012, **116**, 14360–14367.
7 L. Zhang, S. Z. Qiao, Y. G. Jin, Z. G. Chen, H. C. Gu and G. Q. Lu, *Adv. Mater.*, 2008, **20**, 805–809.
8 J. P. Ge, Y. X. Hu and Y. D. Yin, *Angew. Chem., Int. Ed.*, 2007, **46**, 7428–7431.
9 F. Zhang, R. Che, X. M. Li, C. Yao, J. P. Yang, D. K. Shen, P. Hu, W. Li and D. Y. Zhao, *Nano Lett.*, 2012, **12**, 2852–2858.
10 X. Q. Huang, S. H. Tang, B. J. Liu, B. Ren and N. F. Zheng, *Adv. Mater.*, 2011, **23**, 3420–3425.
11 M. Feyen, C. Weidenthaler, R. Güttel, K. Schlichte, U. Holle, A.-H. Lu and F. Schüth, *Chem. – Eur. J.*, 2011, **17**, 598–605.
12 Z. J. Zhang, L. M. Wang, J. Wang, X. M. Jiang, X. H. Li, Z. J. Hu, Y. L. Ji, X. C. Wu and C. Y. Chen, *Adv. Mater.*, 2012, **24**, 1418–1423.
13 J. Liu, H. Q. Yang, F. Kleitz, Z. G. Chen, T. Yang, E. Strounina, G. Q. Lu and S. Z. Qiao, *Adv. Funct. Mater.*, 2012, **22**, 591–599.
14 W. Li and D. Zhao, *Adv. Funct. Mater.*, 2013, **25**, 142–149.
15 (*a*) P. Li, C.-Y. Cao, Z. Chen, H. Liu, Y. Yu and W.-G. Song, *Chem. Commun.*, 2012, **48**, 10541–10543; (*b*) P. Li, C.-Y. Cao, H. Liu, Y. Yu and W.-G. Song, *J. Mater. Chem. A*, 2013, **1**, 12804–12810; (*c*) H. G. Peng, L. Xu, H. Wu, K. Zhang and P. Wu, *Chem. Commun.*, 2013, **49**, 2709–2711.
16 H. Yang, X. Jiao and S. Li, *Chem. Commun.*, 2012, **48**, 11217–11219.
17 Y. Deng, Y. Cai, Z. Sun, J. Liu, C. Liu, J. Wei, W. Li, C. Liu, Y. Wang and D. Zhao, *J. Am. Chem. Soc.*, 2010, **132**, 8466–8473.
18 Q. Zhang, I. Lee, J.-B. Joo, F. Zaera and Y. Yin, *Acc. Chem. Res.*, 2013, **46**, 1816–1824.
19 Z.-A. Qiao, P. Zhang, S.-H. Chai, M. Chi, G. M. Veith, N. C. Gallego, M. Kidder and S. Dai, *J. Am. Chem. Soc.*, 2014, **136**, 11260–11263.
20 P. Zhang, Y. Gong, H. Li, Z. Chen and Y. Wang, *Nat. Commun.*, 2013, **4**, 1593.
21 T. M. Suzuki, T. Nakamura, E. Sudo, Y. Akimoto and K. Yano, *J. Catal.*, 2008, **258**, 265–272.
22 Y. Yang, X. Liu, X. Li, J. Zhao, S. Bai, J. Liu and Q. Yang, *Angew. Chem., Int. Ed.*, 2012, **51**, 9164–9168.
23 (*a*) I. Dodgson, K. Griffin, G. Barberis, F. Pignataro and G. Tauszik, *Chem. Ind.*, 1989, 830–833; (*b*) *Kirk-Othmer Encyclopedia of Chemical Technology*, ed. M. Howe-Grant, Wiley, New York, 1991.
24 M. Chatterjee, H. Kawanami, M. Sato, A. Chatterjee, T. Yokoyama and T. Suzuki, *Adv. Synth. Catal.*, 2009, **351**, 1912–1924.
25 V. Z. Fridman and A. A. Davydov, *J. Catal.*, 2000, **195**, 20–30.
26 (*a*) H. Liu, Y. Li, R. Luque and H. Jiang, *Adv. Synth. Catal.*, 2011, **353**, 3107–3113; (*b*) D. Zhang, Y. Guan, E. J. M. Hensen, L. Chen and Y. Wang, *Catal. Commun.*, 2013, **41**, 47–51.
27 H. Liu, T. Jiang, B. Han, S. Liang and Y. Zhou, *Science*, 2009, **326**, 1250–1252.
28 (*a*) J.-F. Zhu, G.-H. Tao, H.-Y. Liu, L. He, Q.-H. Sun and H.-C. Liu, *Green Chem.*, 2014, **16**, 2664–2669; (*b*) A. Chen, G. Zhao, J. Chen, L. Chen and Y. Yu, *RSC Adv.*, 2013, **3**, 4171–4175.
29 (*a*) Y. Wang, J. Yao, H. Li, D. Su and M. Antonietti, *J. Am. Chem. Soc.*, 2011, **133**, 2362–2365; (*b*) Y. Li, X. Xu, P. Zhang, Y. Gong, H. Li and Y. Wang, *RSC Adv.*, 2013, **3**, 10973–10982.
30 Z. Li, J. Liu, C. Xia and F. Li, *ACS Catal.*, 2013, **3**, 2440–2448.
31 J. Chen, W. Zhang, L. Chen, L. Ma, H. Gao and T. Wang, *ChemPlusChem*, 2013, **78**, 142–148.
32 A. Chen, Y. Li, J. Chen, G. Zhao, L. Ma and Y. Yu, *ChemPlusChem*, 2013, **78**, 1370–1378.